Lifting-Surface Theory for V/STOL Aircraft in Transition and Cruise. II

E. S. LEVINSKY,* H. U. THOMMEN,† P. M. YAGER,‡ AND C. H. HOLLAND‡
Air Vehicle Corporation, San Diego, Calif.

This is the second part of a two-part paper dealing with a large-tilt-angle lifting-surface theory for tilt-wing and tilt-propeller (or rotor) type V/STOL aircraft. Part I presented a new inclined actuator disk theory and a model for slipstream swirl. In Part II, the inclined actuator disk analysis is combined with a discrete-vortex Weissinger-type lifting-surface theory for application to wing-propeller combinations at arbitrary wing angle of attack, propeller tilt angle, and thrust coefficient. Configurations with one, two, or four slipstreams are considered, and effects of slipstream rotation are included in all but the single-slipstream cases. Agreement between theory and experiment is shown to be satisfactory for small slipstream inclination angles. However, at large tilt angles, the theory (with an undeformed, but displaced, slipstream and wake) is shown to predict lower downwash angles in the tail region than observed from a single set of test data, possibly due to slipstream deformation and wake rollup. Use of only one-half the calculated wake displacement is shown to give improved agreement. Insufficient downwash angle data are currently available for making a general evaluation of the theory at large slipstream angles.

Nomenclature

A_p = propeller area
b = wing span
C_l = section lift coefficient based on q_∞
C_{l_a} = section ideal lift coefficient
C''_n = section normal force coefficient based on slipstream total pressure [$= n/c(q_\infty + \Delta H)$]
c = wing chord length
$\mathbf{D}$ = drag force
H = total pressure
h = one-half of the vortex spacing on the wing
i = $(-1)^{1/2}$
J = propeller advance ratio
K = number of slipstreams
$\mathbf{L}$ = lift force
M = number of slipstream control points
$\mathbf{n}$ = normal force per unit span
P = potential influence function
q = dynamic pressure
R = radius of fully contracted slipstream
R_p = propeller radius
r,θ = cylindrical coordinates, slipstream coordinate system
S = downwash velocity influence coefficient
T''_c = propeller thrust coefficient [$= T/A_p(q_\infty + \Delta H)$]
u,v,w = velocity components in slipstream coordinate system
$\mathbf{V}$ = velocity
$\mathbf{V}_\Gamma$ = induced velocity inside slipstream
$\mathbf{V}_\infty$ = freestream velocity
$\mathbf{V}_R$ = resultant velocity
v_θ = swirl velocity
w_∞ = component of freestream velocity in z direction
x,y,z = slipstream coordinate system
x',y',z' = freestream coordinate system
y_p = spanwise position of propeller centerline
$\mathbf{Z}$ = complex variable $Z = re^{i\vartheta} = y + iz$
α = wing angle of attack
α_{eff} = effective angle of attack
α_a = ideal angle of attack
α_p = propeller tilt angle
α_δ = flap effectiveness parameter
Γ = vortex strength
Δ = difference operator
$\Delta\theta_n$ = vortex spacing on slipstream(s)
δ = inclination of slipstream vortex tube with respect to the freestream
δ_f = flap angle, deg
δ_{mn} = Kronecker delta
ϵ = downwash angle
μ = ratio u_o/u_s
ν_t = effective turbulent kinematic viscosity
ρ = density
φ = velocity perturbation potential
φ' = reduced velocity perturbation potential ($= \mu\varphi$)
$\varphi_{o\Gamma},\varphi_{i\Gamma}$ = perturbation potentials due to wing and slipstream horseshoe vortex systems
Ω = effective turbulent origin

Subscripts

a = ideal
i,j = summation indices over wing
k,l = summation indices over the number of slipstreams
m = slipstream control point
m,n = summation indices over the slipstream(s)
o = outside slipstream
p = propeller
R = resultant
s = inside slipstream
Γ = induced by wing and slipstream vortex elements
∞ = freestream

Received December 2, 1968; revision received June 4, 1969. The research was supported by the U.S. Army Aviation Material Laboratories under Contract No. DAAJ02-67-C-0059.

* Vice President. Member AIAA.
† Former Staff Scientist, now Professor with Southeastern Massachusetts Technological Institute, Department of Mechanical Engineering, North Dartmouth, Mass.
‡ Staff Scientist.

I. Wing Lifting-Surface Theory with Inclined Slipstreams

A METHOD will be developed for calculating the span loading and wake flowfield, inside and outside the slipstream, for a wing with inclined slipstreams representative of tilt-wing or tilt-propeller/rotor V/STOL aircraft. The procedure will be applied to aircraft with one, two, or four slipstreams. For reasons of computational simplicity, the plane of the wing will be assumed to pass through the center of the slipstream(s) and to bisect the slipstream into upper and lower halves. Also, for reasons of simplicity, the formulation will be restricted to configurations with symmetrical span loadings about the aircraft centerline. This eliminates consideration of slipstream swirl for single-slipstream aircraft, and requires that the propellers be rotating in opposite

directions on each wing panel for the two- and four-slipstream configurations.

Basically, the method to be developed can be considered a combination of the inclined actuator disk theory developed in Part I[15] and the Ribner and Ellis potential theory for a wing in an uninclined slipstream.[1-3] The approach used, as shown in Fig. 1, replaces the wing by a system of discrete small-span horseshoe vortices with the bound vortex elements placed along the $\frac{1}{4}$-chord line (assumed unswept). The wing vortex system will produce velocity perturbations which in general violate both the pressure and normal velocity boundary conditions across the slipstream interfaces. To correct for the pressure boundary condition, a system of horseshoe vortex elements is also placed around each cylindrical vortex tube representing the boundaries of the slipstream. Violation of the normal velocity boundary condition across the slipstream is automatically suppressed by using a reduced velocity potential $\varphi'_s = \mu\varphi_s$ inside the slipstream, as done by Ribner and Ellis.

The tangential flow boundary condition is satisfied on the wing at the $\frac{3}{4}$-chord points according to the well-known Weissinger lifting-surface theory, e.g., Gray and Schenk.[4] However, the resultant velocity now includes effects of slipstream inclination, swirl, and perturbations from the slipstream horseshoe vortex systems, in addition to perturbations from the wing horseshoe vortex system as in Ref. 4. The pressure boundary condition is satisfied across the slipstream in a linear approximation, as originally suggested by Koning.[5] Satisfaction of the wing and slipstream boundary conditions leads to a system of linear simultaneous equations whose unknowns are the strengths of the wing and slipstream vortex elements. Subsequent solution of this system leads to the span loading and velocity field.

A further simplification has been to take all trailing vortex elements as straight and inclined downward to the free-stream at the same angle δ as the axis of the vortex tube. It is recognized that a somewhat improved model might be to take the direction of the trailing vortices as coincident with the local flow angle at the particular spanwise station. Because of the additional computational complexities, it was decided to forego this remodeling until justified by comparison with experimental data.

In the following sections, expressions are derived for the wing and slipstream boundary conditions in terms of the unknown vortex strengths. Results of the computational procedure are then compared with test data.

Boundary Conditions

The boundary conditions to be satisfied are a constant pressure and a constant normal velocity angle across the slipstream, and tangential flow to the effective airfoil mean line at the $\frac{3}{4}$-chord position of the wing.

Slipstream boundary conditions

The pressure boundary condition, using the incompressible form of the Bernoulli equation, may be expressed as

$$2\Delta H/\rho = [(u_s + u_{s\Gamma})^2 + (v_s + v_{s\Gamma})^2 + (w_s + w_{s\Gamma})^2] - [(u_o + u_{o\Gamma})^2 + (v_o + v_{o\Gamma})^2 + (w_o + w_{o\Gamma})^2]$$

where the single subscripted velocity components are for zero loading on the wing and give the velocity due to slipstream inclination [Eqs. (19) and (20) of Ref. 15]. Quantities with a second subscript Γ refer to perturbations due to the wing vortex system and images. Using the pressure continuity condition across the slipstream boundary [e.g., Eq. (10) of Ref. 15], and also neglecting second-order perturbations in accordance with the usual linearity assumptions, the above expression becomes $u_s u_{s\Gamma} + v_s v_{s\Gamma} + w_s w_{s\Gamma} = u_o u_{o\Gamma} + v_o v_{o\Gamma} + w_o w_{o\Gamma}$. This condition will be satisfied on the slipstream in the region of the wing, for which the first

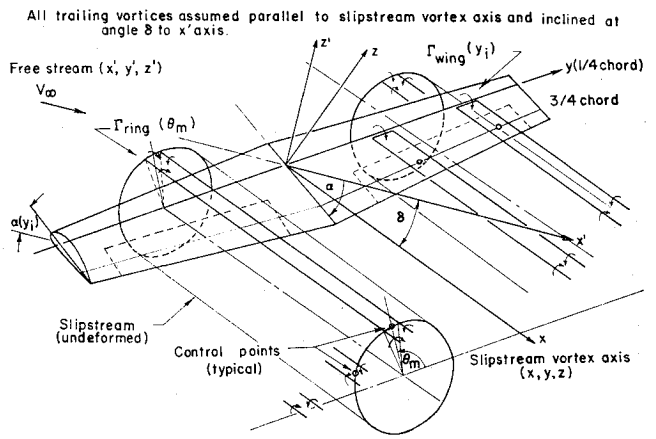

Fig. 1 Vortex singularities for lifting-surface theory with inclined slipstream.

terms on the left- and right-hand sides may be assumed dominant. In terms of the perturbation velocity potentials $\varphi_{s\Gamma}$ and $\varphi_{o\Gamma}$ inside and outside the slipstream, this becomes

$$u_s(d\varphi_{s\Gamma}/dx) \simeq u_0(d\varphi_{o\Gamma}/dx) \tag{1}$$

which is the usual linearized pressure boundary condition originally introduced by Koning.§ Equation (1) should be satisfied for all x in the vicinity of the wing, and at all azimuthal positions θ around the slipstream. However, following Koning and others, Eq. (1) is integrated from $x = -\infty$ to $x = \infty$ giving

$$u_s\varphi_{s\Gamma}(\infty,R,\theta) = u_0\varphi_{o\Gamma}(\infty,R,\theta) \tag{2}$$

where $\varphi_{s\Gamma}(-\infty) = \varphi_{o\Gamma}(-\infty) = 0$. This allows the pressure boundary condition to be satisfied in the Trefftz plane. We note, however, that Eq. (2) satisfies the linearized pressure boundary condition [Eq. (1)] in an average sense only, and is therefore less exact.

The boundary condition on the normal velocities may be readily generalized to include the velocity perturbations due to the wing. Assuming that the axial perturbation velocities are small compared to u_s and u_o, and utilizing Eq. (1) of Ref. 15, we obtain $(\partial\varphi_{o\Gamma}/\partial r)/u_o = (\partial\varphi_{s\Gamma}/\partial r)/u_s$ which can be satisfied on the slipstream $r = R$, for all x and θ by the placement of a suitable distribution of sources and sinks of strength proportional to the normal velocity jump. Following Ribner and Ellis, a reduced potential $\varphi'_{s\Gamma} = (u_o/u_s)\varphi_{s\Gamma}$ is used inside the slipstream, so that the normal velocity jump is suppressed. In terms of $\varphi'_{s\Gamma}$, the pressure boundary condition [Eq. (2)] now becomes $\varphi'_{s\Gamma}(\infty,R,\theta) = (u_0/u_s)^2\varphi_{o\Gamma}(\infty,R,\theta)$. In terms of the potential jump $\Delta\varphi_\Gamma = \varphi_{o\Gamma} - \varphi'_{s\Gamma} = \Gamma(\theta)$, where $\Gamma(\theta)$ is the strength of the horseshoe vortex element on the slipstream at azimuthal angle θ, the pressure condition finally becomes

$$\Gamma(\theta) = (1 - \mu^2)\varphi_{o\Gamma}(\infty,R,\theta) \tag{3}$$

where it is recalled that $\mu = u_o/u_s$.

In the present treatment, Eq. (3) will be satisfied at each of M slipstream control points of azimuthal angle θ_m as shown in Fig. 1. For reasons of simplicity, the formulation will be given for single- and two-slipstream configurations only. Generalization to configurations with four slipstreams is straightforward, and has been incorporated into the machine computational procedure.

Because of the symmetry conditions discussed previously, Eq. (3) need be satisfied only on the starboard wing panel, and θ_m can be limited to the range $0 < \theta_m < \pi$ ($0 < \theta_m < \pi/2$ for a single-slipstream configuration). Thus, we are led to a

§ The full nonlinear pressure condition has been satisfied in the inclined actuator disk theory, Sec. II (Ref. 15).

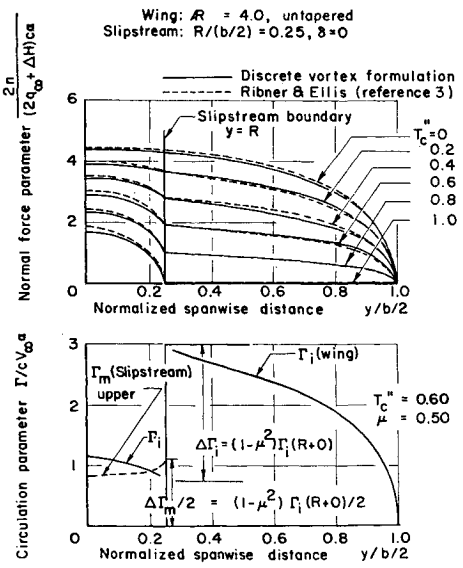

Fig. 2 Comparison of discrete vortex formulation loadings and vortex strength with theory of Ribner and Ellis.

series of M equations of the form

$$\Gamma(\theta_m) = (1 - \mu^2)/2\pi[P_{mj}\Gamma_j + P_{m(-j)}\Gamma_j + P_{mn}\Gamma_n - P'_{mn}\Gamma_n - P'_{m(-n)}\Gamma_n] \quad m = 1,2, \ldots, M \quad (4)$$

where the repeated subscript signifies a summation. The elements P_{mj} represent the contribution to the potential at θ_m, just outside the slipstream, arising from the trailing vortices of the j'th wing horseshoe vortex element of unit strength and centered about $y = y_j$. P_{mj} is obtained from potential theory in terms of complex notation as

$$P_{mj} = \arg(y_j + h_j - Z_m) - \arg(y_j - h_j - Z_m) \quad (5)$$

Here $2h_j$ is the vortex spacing on the wing and $Z_m = y_p + R\exp(i\theta_m)$, where y_p is the coordinate of the slipstream axis. The elements $P_{m(-j)}$ represent the contribution to the potential at θ_m due to the image vortex system on the opposite wing panel, and are obtained from Eq. (5) through the relation

$$P_{m(-j)}(y_j,h_j) = -P_{mj}(-y_j,-h_j) \quad (6)$$

The elements P_{mn} represent the contribution to the potential at θ_m from a pair of trailing vortices of unit strength located on the upper half of the same slipstream at azimuthal angles $\theta_n \pm \Delta\theta_n/2$, and also from their images on the lower half of the slipstream. The vortex pair at $\theta_n = \theta_m$ is included. Because of the symmetry arising when the wing passes through the center of the slipstream, viz., $\Gamma(\theta_n) = -\Gamma(-\theta_n)$, it may be demonstrated that P_{mn} reduces to

$$P_{mn} = \delta_{mn} \quad (7)$$

where δ_{mn} is the Kronecker delta symbol (see Ref. 1). The elements P'_{mn} occur only for multi-slipstream configurations, and represent contributions to the potential from the image vortex system on the upper half of the slipstream of the opposite wing panel. Using potential theory, P'_{mn} may be written as

$$P'_{mn} = \arg[R\exp i(\pi - \theta_n + \Delta\theta_n/2) - R\exp(i\theta_m) - 2y_p] - \arg[R\exp i(\pi - \theta_n - \Delta\theta_n/2) - R\exp(i\theta_m) - 2y_p] \quad (8)$$

Similarly, the $P'_{m(-n)}$ represent contributions from the lower half of the slipstream of the opposite wing panel, and may be obtained from Eq. (8) through the relation

$$P'_{m(-n)}(\theta_n,\Delta\theta_n) = -P'_{mn}(-\theta_n, -\Delta\theta_n) \quad (9)$$

Wing boundary condition

The condition that the resultant flow velocity is tangent to the effective wing surface at the ith control point along the $\frac{3}{4}$-chord line becomes, in the slipstream coordinate system,

$$\tan[(\alpha_{\text{eff}})_i - \delta] = -(w_R/u)_i, \; i = 1,2, \ldots, I \quad (10)$$

Here δ is the inclination of the vortex tube representing the slipstream $(w_R)_i$ is the resultant Z component of velocity, and $(\alpha_{\text{eff}})_i$ is the effective angle of attack of the wing section measured with respect to the remote freestream direction $\mathbf{V}_\infty$. In accordance with thin airfoil theory, we define α_{eff} as the angle of attack of an equivalent flat plate airfoil which yields the same lift coefficient as a cambered and flapped section. Thus, we take

$$\alpha_{\text{eff}} = \alpha - \alpha_a + (\alpha_\delta)\delta_f + C_{l_a}/2\pi \quad (11)$$

where α is the geometric angle of attack and may vary along the span due to geometric and aeroelastic twist, α_a is the ideal angle of attack of the section (the angle at which the pressure at the leading edge of the cambered mean line is finite), α_δ is the section flap effectiveness parameter at zero lift coefficient, δ_f is the flap deflection angle, and C_{l_a} is the ideal lift coefficient, i.e., the lift coefficient at $\alpha = \alpha_a$. The parameters α_a and C_{l_a} are tabulated in Ref. 6 for various airfoil mean lines. The flap effectiveness α_δ is also given in Ref. 6 as a function of the flap/wing chord ratio.

For control points located outside the slipstreams, we take at the i'th station

$$(u)_i = u_0, \qquad (w_R)_i = (w_\Gamma)_i + \sum_{k=1,2,\ldots}^{K} [(w_0 - w_\infty)_k^2]_i + w_\infty \quad (12)$$

where $(w_\Gamma)_i$ is the z component of the velocity induced by all wing and slipstream horseshoe vortex systems at the control point, and w_{ok} is the z velocity component due to the k'th inclined slipstream as obtained from Eq. (19) of Ref. 15. Thus, the multiple slipstream effects on the basic velocity field are approximated by superposition. A complete theory for multiple inclined actuator disks would involve additional interference velocities, inside as well as outside the slipstream, and is not as yet available.

As mentioned in the previous section, a reduced perturbation potential $\varphi'_\Gamma = \mu\varphi_\Gamma$ is used inside a slipstream. In order that the form of Eq. (10) remain invariant across a slipstream boundary, it is required that all other velocity components, i.e., in addition to w_Γ, be reduced by a like factor. Therefore, for control points inside one of the slipstreams, say $k = l$, we take

$$(u)_i = \mu u_s = u_o$$

$$(w_R)_i = \left\{ w_\Gamma + \mu(w_s)_l + \left[\frac{y - y_{pl}}{|y - y_{pl}|}\right](v_\theta)_l + \mu \sum_{k\neq l}^{K} (w_0 - w_\infty)_k \right\}_i \quad (13)$$

Here $(w_s)_l$ is the z velocity component due to inclination inside the l'th slipstream and v_θ is the swirl velocity due to propeller rotation. Expressions for w_s and v_θ are given by Eqs. (20) and (41), respectively, of Ref. 15.

All quantities in Eqs. (10–13) can be regarded as known at a particular control station except for $(w_\Gamma)_i$. Expressing $(w_\Gamma)_i$ in terms of the $\Gamma(y_j)$ and $\Gamma(\theta_n)$ gives

$$(w_\Gamma)_i = S_{ij}\Gamma(y_j) + S_{in}\Gamma(\theta_n) \quad (14)$$

where S_{ij} and S_{in} are influence coefficients which give the z velocity component induced at the i'th control point by wing and slipstream horseshoe vortex elements of unit strength and by their images. Expressions for S_{ij} and S_{in} may be obtained directly from the Biot-Savart law.[7]

Velocity field and downwash angles

Once the strengths of the vortex elements have been obtained, the resultant velocity $\mathbf{V}_R(x,y,z)$ in the flowfield may be found in a straightforward manner. Outside a slipstream, $\mathbf{V}_R$ is found from

$$\mathbf{V}_R = \mathbf{V}_{Ro} = \mathbf{V}_\Gamma(x,y,z) + \sum_{k=1}^{K} [\mathbf{V}_o(y,z) - \mathbf{V}_\infty]_k + \mathbf{V}_\infty \quad (15)$$

where $\mathbf{V}_\Gamma(x,y,z)$ is the resultant velocity induced at the point (x,y,z) in the slipstream coordinate system by all vortex elements on the wing and slipstreams and is obtained from the Biot-Savart law. The velocity contributions from the inclined slipstream are obtained by superposition, as indicated by the summation over k.

Inside a slipstream the induced velocity $\mathbf{V}_\Gamma$ and the vortex elements Γ_j must be augmented by the factor $(1/\mu)$ to correspond to the physical perturbation velocity and vortex strength. We therefore obtain for $\mathbf{V}_R$ inside the l'th slipstream

$$\mathbf{V}_R = (\mathbf{V}_R)_{sl} = \frac{1}{\mu}\mathbf{V}_\Gamma(x,y,z) + \sum_{k\neq l}^{K} [\mathbf{V}_0(y,z) - \mathbf{V}_\infty]_k + [\mathbf{V}_s(y,z)]_l + [v_\theta(y,z)]_l \quad (16)$$

Of importance in the estimation of the static stability and control of V/STOL as well as of conventional aircraft are the dynamic pressure ratio q/q_∞, the downwash angle ϵ and the stability parameter $d\epsilon/d\alpha$. These quantities may readily be found from $\mathbf{V}_R$. For convenience in presentation, we shall express these parameters in freestream coordinates (x',y',z') rather than in the slipstream coordinate system (x,y,z) used in the theoretical development. The two coordinate systems are related by a simple rotation through angle δ as shown in Fig. 1.

The dynamic pressure ratio is given by

$$q(x',y',z')/q_\infty = \mathbf{V}_R \cdot \mathbf{V}_R / V_\infty^2 \quad (17)$$

The resultant downwash angle $\epsilon(x',y',z')$ is defined as the angle which the projection of $\mathbf{V}_R$ in the plane $y' = \text{const}$ makes with $\mathbf{V}_\infty$, and is readily obtained from Eq. (16).

The parameter $d\epsilon/d\alpha$ must be evaluated in a body fixed coordinate system, because the tail is assumed to rotate rigidly with the wing as the angle of attack is changed. Thus, $d\epsilon/d\alpha(x',y',z')$ is evaluated numerically from the expression

$$d\epsilon/d\alpha = [\epsilon(\alpha,x',y',z') - \epsilon(\alpha + \Delta\alpha, x' + \Delta x', y', z' + \Delta z')]/\Delta\alpha \quad (18)$$

where $\Delta x' = z'\Delta\alpha$ and $\Delta z' = -x'\Delta\alpha$.

Resultant force and span loading

Outside the slipstreams, the force per unit span $\mathbf{n}$ may be found from the expression

$$\mathbf{n} = \mathbf{n}_0(y_i) = \rho\Gamma(y_i) \times \mathbf{V}_{R0}(0,y_i,0) \quad (19)$$

where $x = z = 0$ corresponds to the $\frac{1}{4}$-chord line. Inside a slipstream, because of the augmentation of the circulation and induced velocities, we take

$$\mathbf{n} = \mathbf{n}_s(y_i) = \rho(\Gamma(y_i)/\mu) \times \mathbf{V}_{Rs}(0,y_i,0) \quad (20)$$

It should be noted that $\mathbf{n}$ is the resultant of the local lift and induced drag per unit span, because induced velocities have been included in $\mathbf{V}_R$. The direction of $\mathbf{n}$ will vary across the span, and the over-all lift force $\mathbf{L}$ and drag $\mathbf{D}$ may be obtained by integrating the components of $\mathbf{n}$ perpendicular to and parallel to $\mathbf{V}_\infty$ across the span.

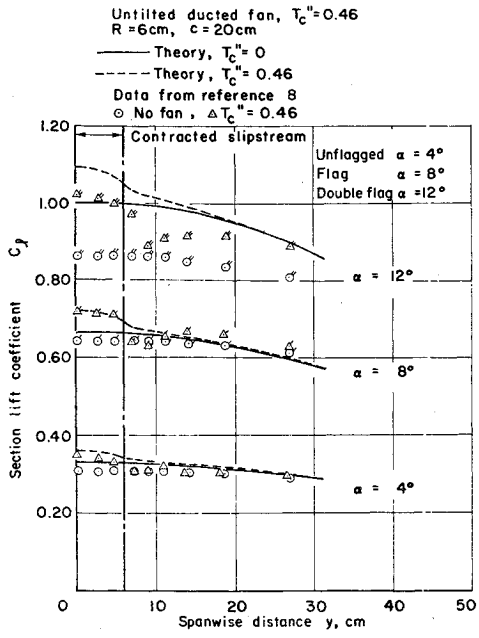

Fig. 3 Comparison of span load distribution with test data, single untilted ducted fan with wing.

The span loading $n(y)$ must be continuous, even across a slipstream interface, because of pressure continuity. The circulation $\Gamma(y_i)$ is therefore discontinuous across the slipstream interface [a similar discontinuity occurs for $\Gamma(\theta_m)$ across the wing[2]]. In the present discrete vortex formulation, $\Gamma(y_i)$ and $\Gamma(\theta_m)$ are not necessarily continuous, and jumps in their values will automatically occur across the slipstream interface as required by the boundary conditions. This is in contrast with the formulation by Ribner and Ellis wherein the jumps in Γ are explicitly prescribed and can unduly complicate the analysis for multiple slipstreams.

FORTRAN computer program

The lifting-surface theory described in Sec. III has been programmed in FORTRAN IV for the CDC 3600 digital computer (32K core). The program was written to handle any wing centered configuration of one, two, or four propellers, provided there is no overlap of the fully contracted slipstreams, and provided the span loading is symmetrical about the airplane centerline. The two- and four-propeller cases allow for slipstream rotation.

The wing has of necessity a straight $\frac{1}{4}$-chord line. However, the chord length, twist, flap-deflection angle, flap-effectiveness, ideal angle of attack, etc., may vary in an arbitrary manner along the span. These spanwise variables are input in a flexible tabular form, and linear interpolation is used throughout. A plotting option can be used to graphically produce curves of wing span loading and contour plots of constant downwash angle, constant dynamic pressure, and a constant derivative of downwash angle with respect to angle of attack. Considerable hand smoothing of the contour plots is usually required, especially near slipstream and wake boundaries.

II. Sample Calculations and Comparison with Data

Several sample calculations have been carried out to compare the present discrete vortex formulation with the calculations by Ribner and Ellis and with experimental data. A comparison of the calculated span load distribution with that

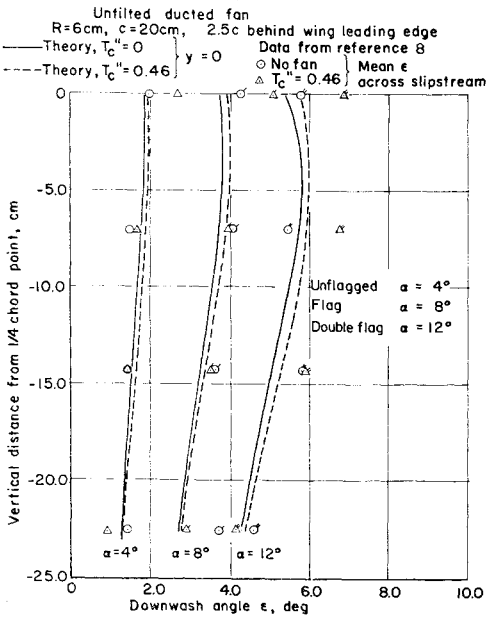

Fig. 4 Comparison of downwash angles with test data, single untilted ducted fan with wing.

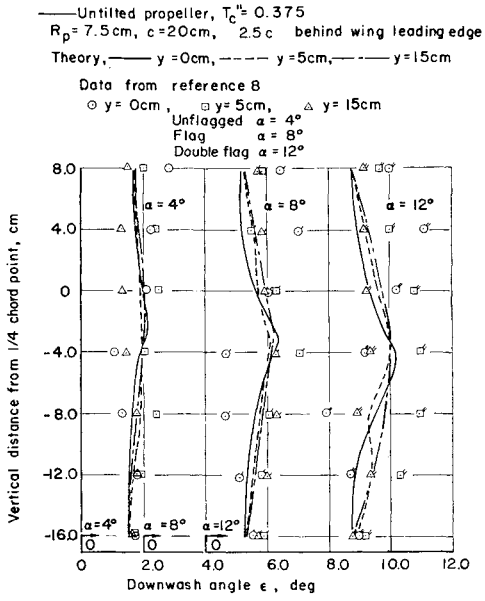

Fig. 6 Comparison of downwash angle with test data, single untilted propeller with wing.

from Ref. 3 is given in Fig. 2 for a wing with a single untilted slipstream. According to Ribner and Ellis, discontinuities in the wing vortex strength are required across the slipstream interface $r = R$ such that $\Gamma(R + 0) - \Gamma(R - 0) = (1 - \mu^2)\Gamma(R + 0)$ whereas a similar jump in slipstream vortex strength is required across the wing. As shown in Fig. 2, jumps of approximately this magnitude were obtained with the discrete vortex formulation.

A comparison of the calculated span loadings and downwash angle with test data by Stüper[8] is found in Figs. 3–7. Shown in Figs. 3 and 4 are the span loading and downwash angle distribution, respectively, for a wing in the slipstream of an untilted ducted fan with straightener vanes to remove swirl effects. Good agreement is found except at $\alpha = 12°$, for which the wing has probably stalled.

A similar comparison, however, for a wing with a single untilted propeller, is given in Figs. 5 and 6. Because the present theory is limited to symmetrical span load distributions, slipstream swirl can only be included for two- and four-propeller configurations. The experimental span loading and downwash data were therefore averaged (right and left wing panels) before being plotted in Figs. 5 and 6 for comparison with theory. Once again, reasonable agreement is found, except for the highest α. A similar span loading comparison, but for a single propeller inclined upward 6° with respect to the wing zero lift angle, is shown in Fig. 7. Again, average experimental data were used.

Although many more test data are available in Ref. 8 for comparison with theory, all data are for relatively small propellers at small inclination angles. Tests of comparable detail but for propeller sizes and tilt angles more representative of V/STOL configurations and operational conditions are required to substantiate the theory.

This requirement has been partially met by the half-model tests of Ref. 9, wherein span loading data were obtained by testing a segmented wing and propeller simulating a two-engine V/STOL aircraft at large tilt angles. A comparison between the present theory, including effects of slipstream

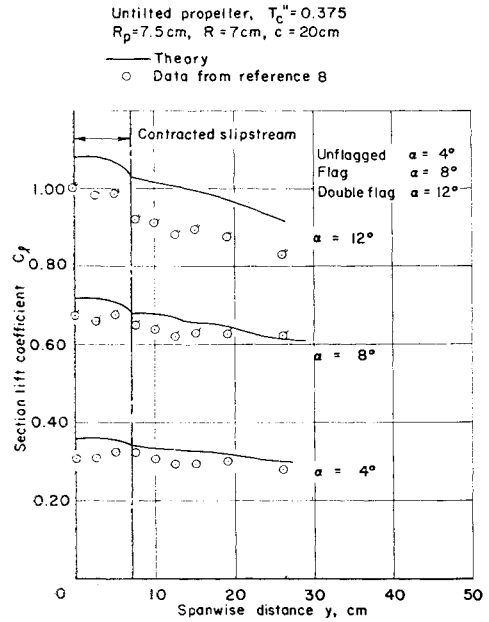

Fig. 5 Comparison of span load distribution with test data, single untilted propeller with wing.

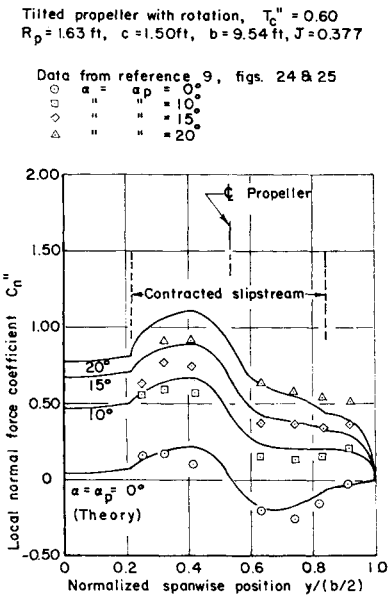

Fig. 7 Comparison of span load distribution with test data, single tilted propeller with wing.

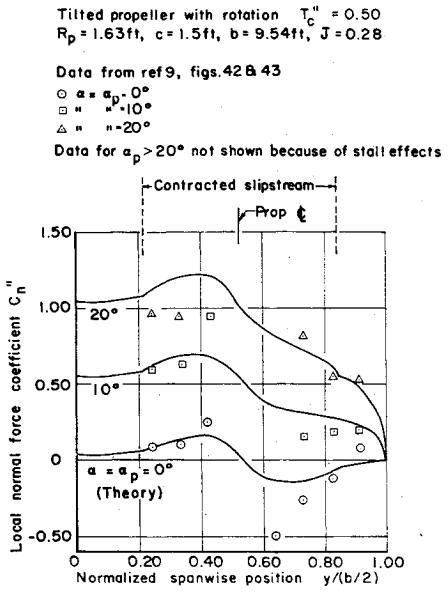

Fig. 8 Comparison of span load distribution with test data: two tilted propellers with rotation, $T''c$ = 0.50.

swirl, and representative data from Ref. 9 is given in Figs. 8 and 9. Satisfactory agreement is shown at angles of attack and propeller inclination angles at or below 20°, for which wing stall effects and wind-tunnel wall interference effects are probably small. The test data at larger incidence angles and for thrust coefficients $T''_c \geq 0.90$ have not been included in the comparison, because stall and wall interference effects have been observed in the data.

Although no general downwash angle survey is available for large tilt angles, i.e., on a scale comparable to that of Ref. 8 at small tilt angles, it is still possible to obtain average values of the downwash angle at the tail location from tail-on and tail-off wind-tunnel test data. Such data (Ref. 10) are compared with the theory in Fig. 10. The test model was a $\frac{1}{11}$-scale version of the XC-142 aircraft. The experimental downwash angle was taken as the tail incidence angle with respect to the remote freestream direction at which both tail-on and tail-off pitching moment coefficients were equal, and represents an average value across the tail span. The theoretical downwash angle was calculated at the location of the horizontal tail $c/4$ line in the plane $y/(b/2) = 0.325$

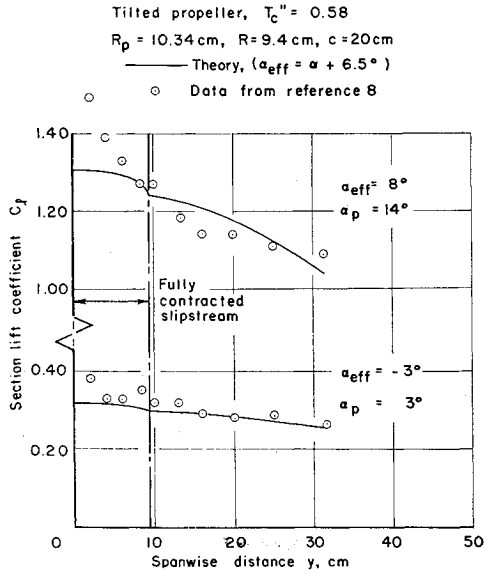

Fig. 9 Comparison of span load distribution with test data: two tilted propellers with rotation, $T''c$ = 0 .60.

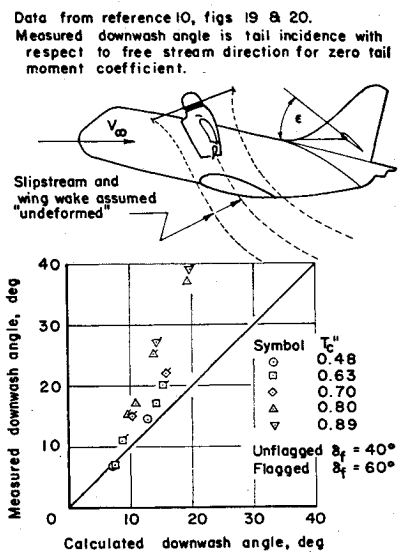

Fig. 10 Comparison of downwash angle with test data: four tilted propellers with rotation, full vertical wake displacement.

(70% of the tail semispan). Corrections were made in the theory for the vertical displacement of the wing wake and of the slipstream interface by shifting these boundaries an amount equal to the calculated displacement of the wing wake (see design charts).

As shown in Fig. 10, satisfactory agreement was found for $\epsilon \lesssim 10°$. For test conditions $(\alpha, T''_c, \delta_f)$ which resulted in downwash angles in excess of 10°, the experimental values for ϵ were significantly greater than calculated from theory. One possible explanation for this disagreement is that the slipstream and wing wake are deformed in such a manner that their downward displacement below the vertical tail is appreciably reduced. Thus, it is known that a completely rolled-up wake is displaced downward by only $2/\pi^2$ of the displacement of a plane vortex wake from an elliptically loaded wing.[11] Although wake roll-up generally occurs behind the tail position at moderate lift coefficients and large aspect ratios, slipstream effects might well accelerate the roll-up process, because of the low effective aspect ratios of the wing segments inside the slipstream. Similar results were noted by Heyson and Katzoff,[12] who observed a very rapid roll-up of the rotor slipstream. They found that the rolled-up vortices had been displaced downward only about one-half as far as the calculated momentum wake.

In lieu of a complete wake theory, which includes slipstream deformation and wake roll-up, it was decided to correct

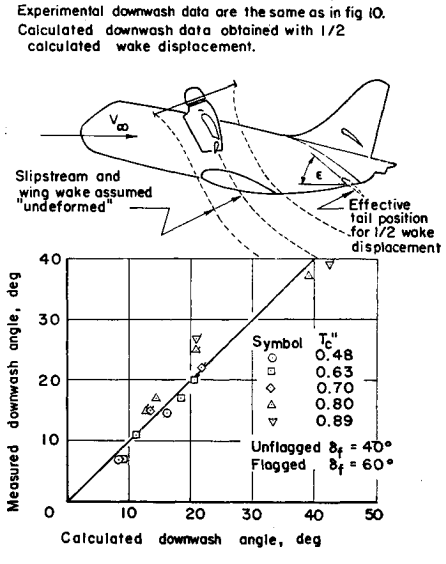

Fig. 11 Comparison of downwash angle with test data: four tilted propellers with rotation, one-half vertical wake displacement.

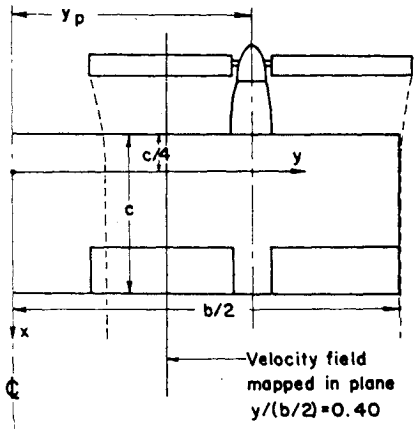

Wing		
Taper ratio	Aspect ratio	Quarter chord sweep
1.0	4.8	0

Flap		
Percent chord	Spanwise extent	Effectiveness
30	16%–54%; 70%–100%	0.6

Propeller			
Diameter to span ratio	Percent b/2 location	Advance ratio	Rotational direction
0.42	62	0.341	inboard down

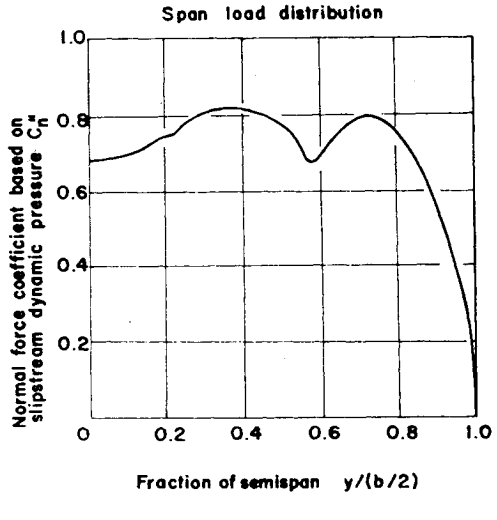

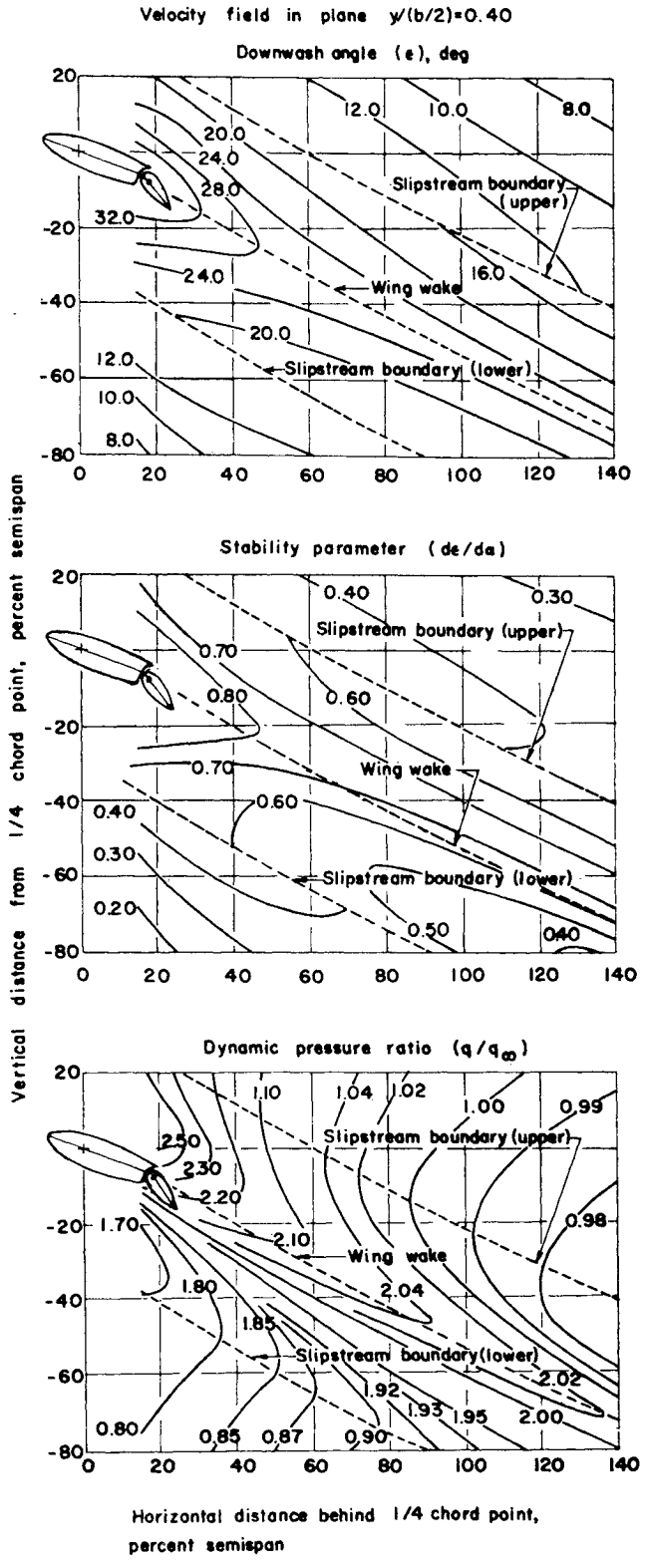

Fig. 12 Two-slipstream configuration design charts: $T''c = 0.5, \alpha = 20°, \alpha_P = 20°, \delta_f = 30°, J = 0.34$.

for these effects by using only one-half of the calculated undeformed wake displacement (or, equivalently, to shift the tail downward by this amount). Substantially improved agreement with the data from Ref. 10 was thereby obtained, as shown in Fig. 11.

Because of the lack of sufficient test data at large tilt angles, it was decided to forego any modification of the theory for slipstream deformation and roll-up effects until further evaluation and comparison with test data could be carried out.

III. Design Charts

Knowledge of the structural, aerodynamic, longitudinal stability and control characteristics of V/STOL aircraft requires knowledge of the span load distribution and of the wake velocity field. In order to supply the aircraft design engineer with data for making a rational estimate of these characteristics, design charts have been prepared for the span loading coefficient $C''_n(y)$, downwash angle ϵ, stability parameter $d\epsilon/d\alpha$, and dynamic pressure ratio q/q_∞ as obtained from the

present lifting-surface theory. The results are presented in Figs. 21–50 of Ref. 13. A typical set of design charts is shown here in Fig. 12.

The design charts were prepared for twin-propeller and four-propeller tilt-wing configurations with and without flaps. The wing and flap planforms and propeller position and size were taken similar to the Canadair CL-84 and the Ling-Temco-Vought XC-142a aircraft for twin- and four-propeller aircraft, respectively. The flight conditions and aerodynamic parameters (e.g., α, α_p, T''_c, δ_f, J, etc.) were chosen as representative of V/STOL aircraft operations in the hover, transitional, and cruise regimes. Thus, the figures may be considered an extension of the cruise design charts by Silverstein and Katzoff[14] to conditions wherein inclined slipstream effects are of significance.

The data for the charts were obtained from the computer program described in Sec. II. Running time was approximately 30 sec/case. Considerable data smoothing was required, because the discrete vortex formulation gives spurious results at points near the singularities. The contour plots are presented in the freestream coordinate system (x', y', z').

It is noted that no wake roll-up or slipstream distortion effects are included. However, because of the large angles of attack, effects of the vertical displacement of the wake have been approximated by shifting the contour plots by an amount $\Delta z(x,y)$ where

$$\Delta z = \int_0^x w_R(x,y,0)dx$$

This results in both the slipstream boundaries and wing vortex wake being displaced downward by an amount equal to the displacement of the wing vortex wake. As pointed out in the previous section, slipstream deformation and wake roll-up may reduce the vertical displacement from that shown in the design charts.

The design charts include the effects of slipstream rotation, with viscous core effects reducing the swirl velocities to zero along the streamline passing through the propeller axis [Eq. (41) of Ref. 15]. All computations were made with an effective turbulent viscosity $\nu_t = 0.10$ ft^2/sec, as obtained from wind-tunnel data,[15] with no scaling for aircraft size. The effective turbulent origin Ω used in Eq. (41) was taken as 200 ft. and 400 ft. for the two- and four-slipstream configurations, respectively.

IV. Conclusions

A theory has been developed for an inclined actuator disk which satisfies the normal velocity and nonlinear pressure boundary conditions. This theory has been used as the basis for the development of a wing lifting-surface theory with inclined slipstreams for application to V/STOL aircraft in the transitional regime. The lifting-surface theory has been programmed on the CDC 3600 digital computer. Sample calculations have been carried out to compare with available test data and also to present design charts of span loading, downwash angle, $d\epsilon/d\alpha$, and dynamic pressure in the wake for typical V/STOL aircraft.

Comparison with test data has shown that the theory predicts the span loading and downwash angle reasonably well for small angles of attack and small propeller tilt angle. However, at large tilt angles, the theory (with an undeformed, but displaced, slipstream and wake) tends to predict significantly lower downwash angles in the tail region than observed from a single set of test data, possibly due to slipstream deformation and wake roll-up which tend to reduce the downward wake displacement. Use of only one-half of the calculated wake displacement gave improved agreement with measured downwash angles at these conditions. However, the lack of sufficiently detailed test data for conditions representative of V/STOL transition makes evaluation of the theory and assessment of its limitations difficult.

References

[1] Ribner, H. S., "Theory of Wings in Slipstream," Rept. 60, 1959, University of Toronto, Institute of Aerophysics.

[2] Ellis, N. D., "A Computer Study of a Wing in a Slipstream," TN 101, 1967, University of Toronto, Institute for Aerospace Studies.

[3] Ribner, H. S. and Ellis, N. D., "Theory and Computer Study of a Wing in a Slipstream," AIAA Paper 66–466, Los Angeles, Calif., 1966.

[4] Gray, W. L. and Schenk, K. M., "A Method for Calculating the Subsonic Steady-State Loading on an Airplane with a Wing of Arbitrary Planform and Stiffness," TN 3030, 1953, NACA.

[5] Koning, C., "Influence of the Propeller on Other Parts of the Aircraft Structure," *Aerodynamic Theory*, Vol. IV, Div. M, edited by W. F. Durand, Dover, New York, 1935, pp. 361–431.

[6] Abbott, I. A. and von Doenhoff, A. E., *Theory of Wing Sections*, Dover, New York, 1959.

[7] Glauert, H., *The Elements of Aerofoil and Airscrew Theory*, Cambridge University Press, 1947, pp. 157–160.

[8] Stüper, J., "The Effect of Propeller Slipstream on Wing and Tail," TM 874, 1938, NACA.

[9] George, M. and Kisielowski, E., "Investigation of Propeller Slipstream Effects on Wing Performance," TR 67-67, 1967, U. S. Army Aviation Materiel Labs.

[10] Goodson, K. W., "Longitudinal Aerodynamic Characteristics of a Flapped Tilt-Wing Four-Propeller V/STOL Transport Model," TN D-3217, 1966, NASA.

[11] Helmbold, H. B., "Limitations of Circulation Lift," *Journal of the Aeronautical Sciences*, Vol. 24, No. 3, March 1957, pp. 237–238.

[12] Heyson, H. H. and Katzoff, S.: "Induced Velocities Near a Lifting Rotor with Nonuniform Disk Loading," TR 1319, 1957, NASA.

[13] Levinsky, E. S. et al., "Lifting Surface Theory and Tail Downwash Calculations for V/STOL Aircraft in Transition and Cruise," TR 68-67, Oct. 1968, U S. Army Aviation Materiel Labs.

[14] Silverstein, A. and Katzoff, S., "Design Charts for Predicting Downwash Angles and Wake Characteristics Behind Plain and Flapped Wings," TR 648, 1938, NACA.

[15] Levinsky, E. S. et al., "Lifting-Surface Theory for V/STOL Aircraft in Transition and Cruise. I." *Journal of Aircraft*, Vol. 6, No. 6, Nov.–Dec. 1969, pp. 488–495.